New lifetime measurements in ^{109}Pd and the onset of deformation at $N = 60$

B. Bucher,[1,2,*] H. Mach,[1,3,†] A. Aprahamian,[1] G. S. Simpson,[4] J. Rissanen,[5,‡] D. G. Ghiţă,[6] B. Olaizola,[7,§] W. Kurcewicz,[8] J. Äystö,[5,‖] I. Bentley,[1,9] T. Eronen,[5,¶] L. M. Fraile,[7] A. Jokinen,[5] P. Karvonen,[5,#] I. D. Moore,[5] H. Penttilä,[5] M. Reponen,[5] E. Ruchowska,[3] A. Saastamoinen,[5,¶] M. K. Smith,[1] and C. Weber[5,**]

[1]*Department of Physics, University of Notre Dame, Notre Dame, Indiana 46556, USA*

[2]*Lawrence Livermore National Laboratory, Livermore, California 94550, USA*

[3]*Division of Nuclear Physics, BP1, National Centre for Nuclear Research, ul. Hoża 69, 00-681, Warsaw, Poland*

[4]*LPSC, Université Joseph Fourier Grenoble 1, CNRS/IN2P3, Institut National Polytechnique de Grenoble, F-38026 Grenoble Cedex, France*

[5]*Department of Physics, University of Jyväskylä, P.O. Box 35, FI-40014 Jyväskylä, Finland*

[6]*National Institute for Physics and Nuclear Engineering, R-77125 Bucharest-Magurele, Romania*

[7]*Grupo de Física Nuclear, Facultad de Físicas, Universidad Complutense – CEI Moncloa, E-28040 Madrid, Spain*

[8]*Faculty of Physics, University of Warsaw, Pasteura 5, PL 02-093 Warsaw, Poland*

[9]*Department of Chemistry and Physics, Saint Mary's College, Notre Dame, Indiana 46556, USA*

(Received 15 October 2015; published 14 December 2015)

Several new subnanosecond lifetimes were measured in ^{109}Pd using the fast-timing $\beta\gamma\gamma(t)$ method. Fission fragments of the $A = 109$ mass chain were produced by bombarding natural uranium with 30 MeV protons at the Jyväskylä Ion Guide Isotope Separator On-Line (IGISOL) facility. Lifetimes were obtained for excited states in ^{109}Pd populated following β decay of ^{109}Rh. The new lifetimes provide some insight into the evolution of nuclear structure in this mass region. In particular, the distinct structure of the two low-lying $7/2^+$ states occurring systematically across the Pd isotopic chain is supported by the new lifetime measurements. The available nuclear data indicate a sudden increase in deformation at $N = 60$ which is related to the strong p-n interaction between $\pi g_{9/2}$ and $\nu g_{7/2}$ valence nucleons expected in this region.

DOI: 10.1103/PhysRevC.92.064312 PACS number(s): 29.30.Kv, 27.60.+j, 23.20.−g, 21.10.Tg

I. INTRODUCTION

Neutron-rich nuclides in the mass region $A \sim 110$ display a wealth of interesting structural phenomena. This region is characterized by the rapid onset of deformation, isomerism, triaxiality, and shape coexistence, to name a few (e.g., Refs. [1–17]). The precise origins and evolutions of such phenomena are still not well understood. The persistence or disappearance of shells and subshells in this region can have significant impacts on the radioactive decay rates of nuclei, while the presence of deformation-driving orbitals can lead to extended shapes.

In the past, it has been difficult to study unstable nuclei in this mass region in much depth due to low production rates. However, even with the higher production rates available from the current and next generation radioactive ion beam facilities, the primary experimental emphasis has been on the most neutron-rich isotopes in an effort to ascertain the properties of the coveted r-process nuclides. But before we can make reliable predictions about the structure of neutron-rich nuclei, it is important to understand very well the structure of nuclides nearer to stability.

One of the best probes for revealing nuclear structure information is provided through γ spectroscopy and associated lifetime measurements. While much information now exists in the $A \sim 110$ region on level energies, spins, parities, and decay branchings, lifetimes of excited levels just one or two nuclides from stability remain elusive. Precise measurements of short lifetimes require carefully calibrated detection systems which include high-efficiency γ-ray detectors with good timing and energy resolution. These lifetime measurements rely on multiple coincident events within the detection system. Consequently, sufficient precision is achieved when the production rate of these nuclides is high enough to overcome the resultant loss in efficiency.

In the $A \sim 110$ region, there are relatively few lifetime measurements of nuclear excited states shorter than ∼10 ns. The investigation reported here is part of a large systematic study of lifetimes in this mass region [18]. The previous part of this study focused on the even-mass chains in this region where some of the first results were reported for ^{106}Ru [19] and ^{122}Cd [20]. In this paper we report on the first results from the odd-mass measurements of the $A = 109$ chain. For mass 109, lifetime measurements were made for excited states in ^{109}Tc, ^{109}Ru, ^{109}Rh, and ^{109}Pd. Eight new lifetime measurements of levels in ^{109}Pd are reported, with a discussion on more collective excitations in the odd-A Pd isotopes via the $7/2^+$ and $5/2^+$ levels characteristic of all the Pd nuclei from $A = 97$

*bucher3@llnl.gov

†Deceased.

‡Present address: Fennovoima Oy, Salmisaarenaukio 1, FI-00180 Helsinki, Finland.

§Present address: Physics Department, University of Guelph, 50 Stone Rd E, Guelph, Ontario N1G 2W1, Canada.

‖Present address: Helsinki Institute of Physics, P.O. Box 64, FI-00014 University of Helsinki, Finland.

¶Present address: Cyclotron Institute, Texas A&M University, College Station, Texas 77843, USA.

#Present address: Fortum Power Division, P.O. Box 100, FI-00048 Fortum, Finland.

**Present address: Faculty of Physics, Ludwig-Maximilians University Munich, Am Coulombwall 1, D-85748 Garching, Germany.

to 113. Note that the ground-state spins and parities for the Pd isotopes in this mass range are all $5/2^+$. Of particular interest from a nuclear structure standpoint are the $7/2^+$ states, which appear in pairs at relatively low energies systematically across the Pd isotope chain [21–30] and seem to display two distinct structures. Other levels of interest are the lowest $7/2^-$, which is the only negative-parity state strongly populated in the β decay of ^{109}Rh, and the $5/2_2^+$ state, which has a dominant β-feeding intensity systematically across the Pd isotopic chain [21,25–30]. These $7/2$ and $5/2$ levels are all discussed in Sec. IV. The experimental and analysis details are provided in Secs. II and III, respectively. Section V provides a summary and conclusions.

II. EXPERIMENT

The experiment was performed at the Ion-Guide Isotope Separator On-Line (IGISOL) facility at the University of Jyväskylä, Finland. At IGISOL, isotopes are produced from the fission of natural uranium induced by a 30 MeV proton beam on a thin target. The fission fragments are stopped in a He gas catcher and a common charge state of 1^+ is achieved by virtue of the high first ionization potential of helium (for details see Ref. [31]). After extraction from the gas cell, fragments and other charged impurities are guided into high vacuum via an rf sextupole device [32]. Following electrostatic acceleration to 30 kV, the ions are mass-separated using a dipole sector magnet. The resulting beam of isobars was then focused onto an aluminum catcher where a detection station was set up downstream from the focal plane of the mass separator.

In this experiment, data for the mass chains 105, 107, 109, and 111 were collected with results from $A = 109$ presented in this report. A continuous beam of isobars was deposited on the catcher in a saturation mode. A 3-mm-thick plastic NE111A scintillator was placed directly behind the catcher to record β events. Two high-purity germanium (HPGe) detectors of about 50% relative efficiency were placed on each side (at 90°) of the catcher to record the ensuing γ-decay events following each β decay.

To measure the lifetimes associated with these decays, the advanced time-delayed method $\beta\gamma\gamma(t)$ was used [33–35]. Coincidences between a fast-response β detector and a pair of $LaBr_3$(Ce) detectors, placed above and below the catcher (at 45° relative to the upstream direction), provided excellent timing resolution for the lifetime measurements. The two $LaBr_3$ crystals, one large and one small, were cylindrical in shape. The smaller one was 1 inch long with a 1 inch diameter, while the larger one was 1.5 by 1.5 inches. Each was wrapped around the sides with a few millimeters of lead foil to shield from γ rays that were cross-scattered between detectors.

In this setup, triple coincidences ($\beta\gamma\gamma$) were required to trigger the data acquisition. The recorded events consisted of the various combinations of β-$LaBr_3$-Ge and β-Ge-Ge coincidences. The latter provides clean coincidence spectra for determination of the precise decay path within the daughter nucleus, while the former provides the lifetime measurement once the decay path has been identified. A fast time-to-amplitude converter (TAC) was paired with each of the $LaBr_3$ detectors to extract the lifetimes with the start input coming from the β plastic scintillator and the stop input from the $LaBr_3$ γ signal. The fast TACs had a range of 50 ns, while a time gate of 500 ns was used for the β-Ge coincidence requirement. This meant that lifetimes longer than about 10 ns could not be measured with high precision, and decays populating microsecond isomers (or longer) were mostly cut out from the acquisition system. However, lifetime measurements of such long-lived isomers already exist from previous studies [28]. The purpose of the present work is to provide new lifetime information for the shorter-lived states.

III. ANALYSIS AND RESULTS

Data were recorded over a period of 2 days. The detector gains were monitored for changes by dividing the whole data set into 2-hour time intervals and checking the positions of various peaks in the spectra within these intervals. Any gain shifts found were corrected. The data were then sorted by events according to the hit-pattern (i.e,. β-Ge1-Ge2, β-LaBr1-Ge1, β-LaBr1-Ge2, etc.). Coincidence gates were chosen based on the most prominent peaks in the Ge spectra. Initially some 92 gates were set with eventual addition of numerous other supplementary gates. The coincidence events observed for γ-ray transitions in ^{109}Pd were found to be consistent with the decay scheme and branching intensities of Ref. [28] within the uncertainties of the measurement. However, most spectra did contain a number of contaminant lines due to overlapping γ-ray energies from other nuclides in the mass chain (i.e., ^{109}Rh and ^{109}Ru), including many new γ rays, most of which seem to belong to ^{109}Ru. Favorable peaks for the timing analysis were identified in the coincidence spectra based on statistics and cleanliness (i.e., no doublets). Appropriate projections were then made in the $LaBr_3$ spectra to confirm the availability of timing information for such events. In some cases, despite having sufficient energy resolution in the Ge coincidence spectra, clean time spectra could not be extracted due to the poorer energy resolution from $LaBr_3$ (3% at 662-keV ^{137}Cs line).

The fast-timing analysis has followed our standard procedures. Details of the present analysis are given in Ref. [36]. The analyses include standard corrections for the residual β-walk curve as well as corrections for small drifts in the fast-timing electronics during the measurement. In the first step of the fast-timing analysis we have identified those levels which have long lifetimes that can be measured by the *slope* (deconvolution) method [33]. Such a lifetime is identified by observing an asymmetry, or a tail, on the time-delayed part of the time spectrum. The time spectra are generated by setting appropriate gates on the full energy peaks in the $LaBr_3$ coincidence spectra extracted from the β-LaBr-Ge data. Proper corrections were made for the small Compton background observed in each $LaBr_3$ gate which is present below the full energy peak. The time spectrum is then slope-fitted using a deconvolution technique to separate the prompt time response from the level lifetime [33]. Figure 1 provides an example with the various spectra highlighting the main steps in the analysis procedure.

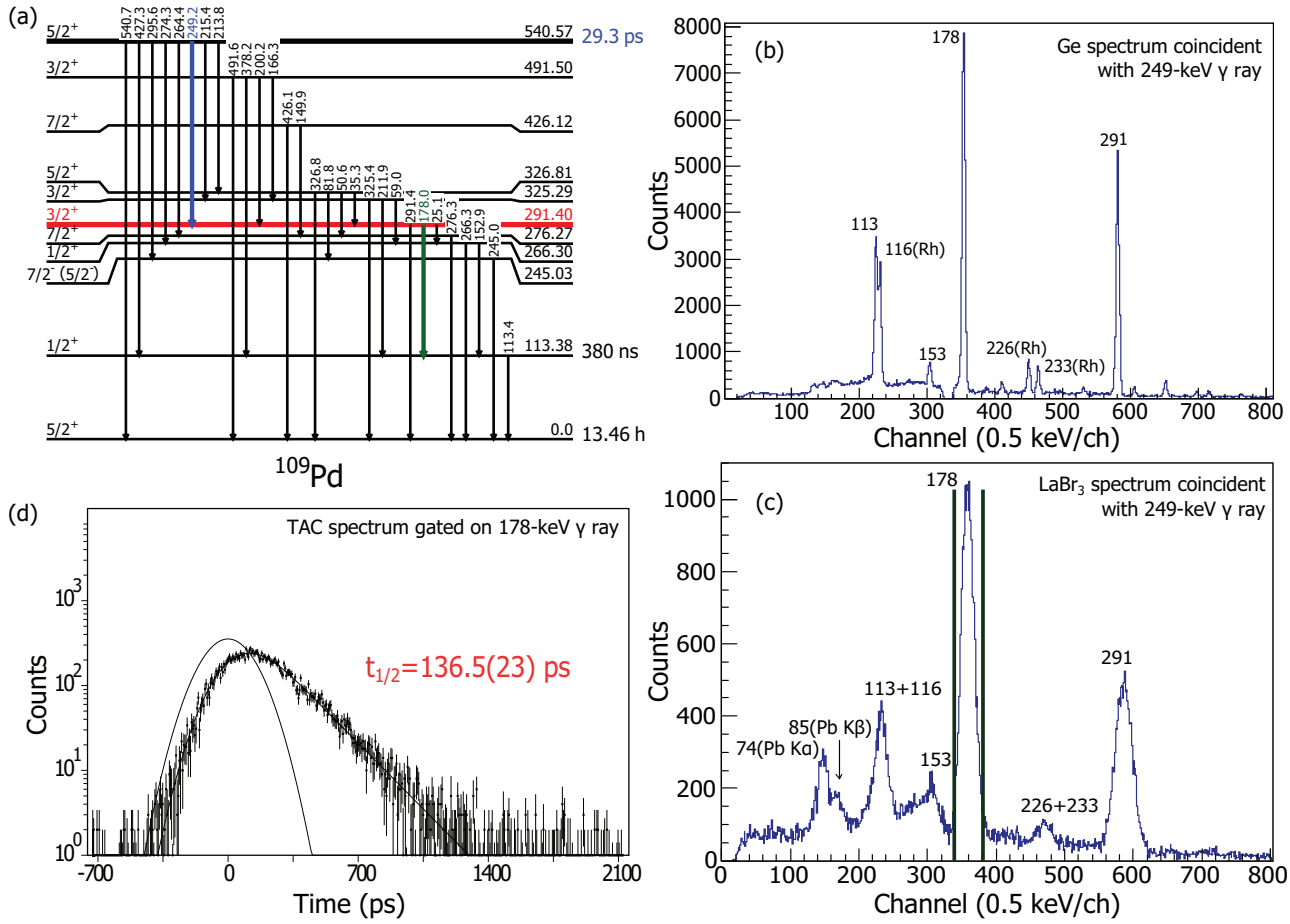

FIG. 1. (Color) An example of the analysis procedure for slope fitting. (a) A gate is placed in the Ge data on the 249-keV γ ray deexciting the 541-keV level (blue). The coincidence spectrum in the opposite Ge is shown in (b). To measure the lifetime of the 291-keV level below, a gate in the $LaBr_3$ on the coincident 178-keV γ ray is placed (c) and projected in the TAC spectrum (d). The TAC spectrum includes the delay from the 541-keV level lifetime. In this case, however, that lifetime is short compared with the lifetime of the 291-keV level and does not influence the observed slope [33]. The fit is shown by the black solid line along with the corresponding prompt time peak (light gray).

For levels where the lifetime was too short to be determined by the deconvolution procedure, the *centroid-shift* method [33] has been used. The time response curves, i.e. calibration curves, were determined for the full-energy-peaks (FEP) and Compton events using known γ-ray energies and level lifetimes in the $A = 138$ β-decay chain, primarily from the β decay of ^{138}Cs to ^{138}Ba (Fig. 2). For γ-ray energies greater than 400 keV, any differences between the two curves are small compared to the measurement uncertainties. However, γ rays with energies below 400 keV display clearly different time responses depending on the nature of the interaction inside the detector [35]. As seen from Fig. 2, background Compton events are delayed relative to FEP events, particularly strongly at the energy of ~220 keV due to a large component of backscattering from surrounding materials. With this information, the energy dependence of the background component in each time spectrum is corrected prior to subtraction, and the resultant time peak due to the FEP event is compared with the baseline curve established by the mass-138 peaks (which have been corrected for their corresponding lifetimes). Any delay relative to the baseline must be due to an associated lifetime for the corresponding level in ^{109}Pd.

The shape of the response curve was well-established from the mass-138 measurements, however the absolute normalization is not since the total delay may be different depending on the β-decay characteristics and how the β-walk correction is done for each mass chain. The absolute normalization is obtained from the two transition pairs 291-249 keV and 178-249 keV that connect the 291-keV and 541-keV levels in ^{109}Pd with delay resulting solely from the 541-keV level lifetime which was extracted from the deconvolution fitting. That is, a gate is placed on each of the 178-keV and 291-keV γ rays in either HPGe detector while a second gate is placed in the $LaBr_3$ spectra on the 249-keV γ ray. The time projection of one of these gates is shown in Fig. 3. Since the 541-keV level in ^{109}Pd is directly fed by the β decay of the ^{109}Rh parent, with negligible feeding to higher levels [28], the time peak centroid of Fig. 3 is delayed relative to the prompt time position solely due to the 541-keV level lifetime. Moreover, due to the high statistics for these two coincidence pairs, it is also possible

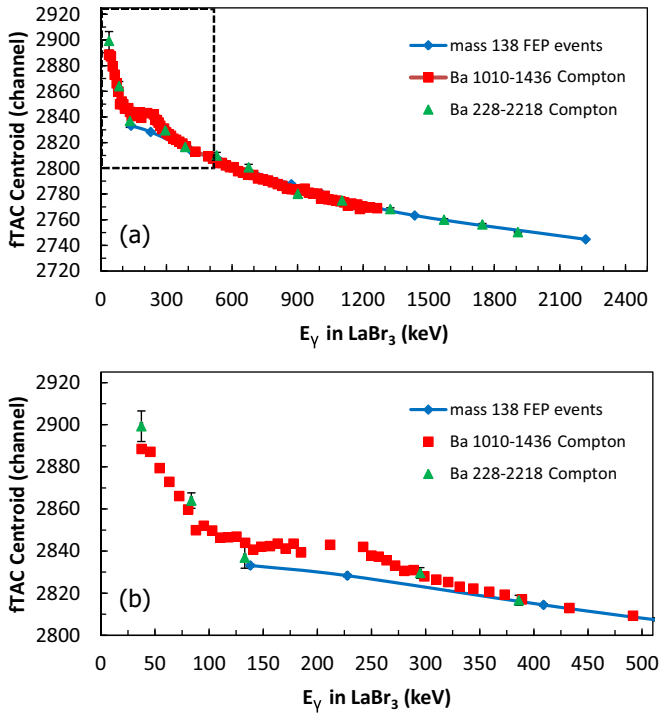

FIG. 2. (Color online) (a) The γ-walk curve generated by events from mass-138 β decays. The blue diamonds represent full-energy-peak (FEP) events, while the red squares and green triangles represent background events (primarily Compton events from the 1436-keV and 2218-keV γ rays in ^{138}Ba). (b) Below 400 keV, background events begin to display a significant delay relative to full-energy events. Peak and background centroid corrections are made separately according to their respective walk curves.

to separate the delayed component of the time spectrum from the prompt component by the slope-fitting method (Fig. 3). The half-life obtained by the slope method is consistent with the value obtained from the centroid-shift analysis for the other available γ pairs depopulating the 541-keV level (i.e., 245-296 keV and 325-215 keV; see Fig. 4). In other words, the time peak centroids for these γ-ray pairs display delays, based on their positions in energy on the γ-walk curve (Fig. 2), which are consistent with the fitted lifetime of the 541-keV level. A further check of the 541 level lifetime and calibration of the absolute prompt time peak positions is provided by using the slope-fitting result for the 113(Ge)-378($LaBr_3$) γ pair [$T_{1/2} = 59(10)$ ps], which gives the half-life for the 492-keV level, as the absolute delay from the prompt position. When this is done, the resultant centroid-shift analysis of the the 541-keV level (using the same γ pairs as mentioned above) gives a half-life in agreement with the original slope-fitting result within 1.1σ. This provides confidence that the deconvolution fit gives an accurate half-life for the 541-keV level, and therefore a reliable calibration of the normalization for the time-response curve used in the centroid-shift analysis.

Eight half-lives were obtained from this measurement. These results are displayed in Table I. One of these level half-lives is for the $5/2_2^+$ level at 327 keV which had been measured previously [14], but with much less precision

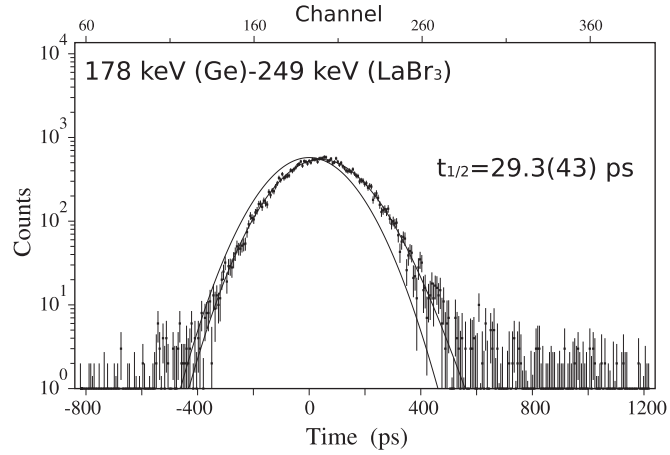

FIG. 3. Deconvolution fitting of the time spectrum from the 249-keV γ ray detected in the large $LaBr_3$ detector in coincidence with the 178-keV γ ray detected in either HPGe. The fitted half-life is in good agreement with the centroid-shift analysis. The prompt time peak from the fit is also displayed (light gray).

[$T_{1/2} = 0.57(15)$ ns]. The value we report here agrees within 2σ with much improved precision. To calculate reduced transition probabilities $B(M\lambda)$, γ-ray branching intensities were taken from Refs. [37,38]. In many cases, the transition multipolarities ($M1/E2$ ratios) were determined from conversion-electron coefficients measured in Ref. [38]. For γ rays with energies less than 90 keV, the $M1/E2$ mixing ratios and intensities were taken from Ref. [37]. It is worth mentioning that none of these low-energy transitions were adopted in the evaluation of Ref. [28], but all are confirmed in this measurement. For transitions where the conversion coefficients had not been measured, the multipolarity was assumed to be purely of the lowest allowed order (e.g., for $\Delta J = 1$ and no change in parity, the transition was assumed to be pure $M1$). For consistency, all conversion coefficients used to derive the transition probabilities were calculated using the BRICC conversion calculator [39]. The only exception to this was for the 25-keV transition from the 291-keV level. Since the transition energy is so close to the Pd K-shell electron binding energy (24.35 keV), the BRICC calculator was unable to calculate the K-shell conversion coefficient, nor does an experimental value exist. Kanazawa *et al.* do provide an upper limit for the $E2$ strength, presumably by measuring the L-shell and/or M-shell conversion coefficients [37]. By measuring the total intensity through γ-γ coincidences, they establish a rough γ-ray intensity which was adopted here. However, other than the $E2$ fraction, no other numbers are provided in that paper. In order to calculate the strengths for the transitions from the 291-keV level, we use our γ-γ coincidence measurements to determine the total 25-keV transition intensity ($I_\gamma + I_{ce}$).

The total intensity was determined by gating on the 249-keV γ ray depopulating the $5/2^+$ level at 541 keV. The efficiency-corrected intensities of the coincident γ rays at energies 291, 178, 266, and 153 keV were compared. The sum of these four (after correction for conversion-electron intensities) gives the total feeding intensity to the 291-keV level (see Fig. 4). The sum of the 266-keV and 153-keV γ

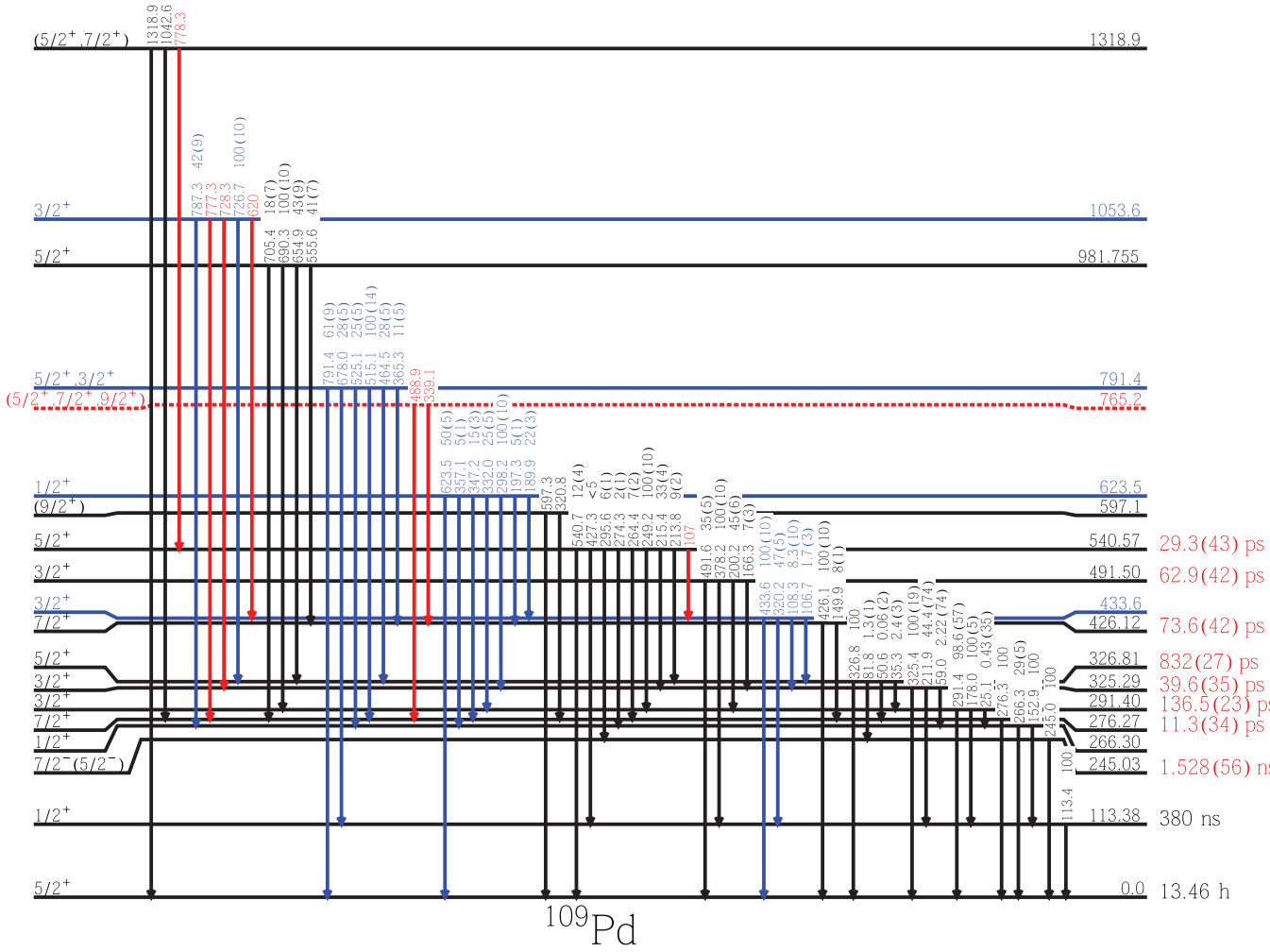

FIG. 4. (Color) ^{109}Pd level scheme with levels observed in $\beta\gamma\gamma$ coincidences after ^{109}Rh decay. Intensities were derived from Refs. [37,38]. Blue levels and γ rays have been observed in the earlier ^{108}Pd(n,γ) experiment by Casten *et al.* [38], but are new to the β-decay scheme. Red levels and γ rays are observed for the first time.

rays gives the intensity through the 25-keV transition from the 291-keV level. The total intensity ratio, $I_{25}/(I_{291}+I_{178})$, was used in the strength calculations for the transitions from the 291-keV level provided in Table I. The experimental value was found to be 0.0324(50). It is important to point out that the experimental γ-intensity ratio between the 291-keV and 178-keV transitions measured in this experiment was in good agreement with the values adopted in Ref. [28]. The γ-intensity ratio between the 266-keV and 153-keV transitions measured here was consistent within experimental uncertainties with the value measured by Kanazawa *et al.* [37], but not consistent with the value measured by Casten *et al.* [38]. Our value for the intensity of the 266-keV γ ray per 100 γ rays of 153 keV is 64(13), while those previous measurements recorded 41.7(90) [37] and 28.9(41) [28,38], respectively.

The level scheme obtained from the analysis of Ge-Ge events is shown in Fig. 4. Five new levels and associated γ rays (colored blue and red in the figure) were added to the β-decay scheme of ^{109}Pd based on the γ-γ coincidence results. The other levels (black) were observed in earlier measurements by Fettweis and Marmol [40] and Kanazawa *et al.* [37] and verified in this experiment. Four of the five new levels were observed in the ^{108}Pd(n,γ) experiment by Casten *et al.* [38], however one new level has been added at 765 keV with two γ rays of energies 489 and 339 keV depopulating it as well as five additional new γ rays distributed between the previously observed levels at 1319, 1054, and 541 keV. Measured β-feeding and γ-ray intensities have not been provided due to the difficulty for this experiment to provide precise values as a result of the triple coincidence requirement. New half-lives have been measured for eight of the low-lying levels above the first-excited 380 ns isomer at 113 keV as shown in Fig. 4 and Table I.

IV. DISCUSSION

There are two $7/2^+$ states that exist at low excitation energies across the Pd isotope chain [21–30] and display two distinct structures which are of particular interest to us. These along with the lowest $7/2^-$, which is the only negative-parity state strongly populated in the β decay of ^{109}Rh, and the $5/2_2^+$ state, which has a dominant β-feeding intensity systematically across the Pd chain [21,25–30], are highlighted below.

TABLE I. Measured half-lives with transition strengths for observed transitions. Multipolarities in square brackets are assumed. Intensities (I_γ) and $M1/E2$ ratios are taken from Ref. [37,38]. The $M1/E2$ ratios are based on measurements of various K-, M-, and L-shell electron conversion coefficients. The *total* conversion coefficients ($\alpha_{\rm tot}$) displayed in the table and used to determine the $B(M\lambda)$'s were calculated using the BRICC conversion calculator [39].

$E^{\rm i}$(keV)	J^π	$T_{1/2}$ (ps)	E_γ(keV)	I_γ	$E^{\rm f}$(keV)	J^π	$M\lambda$	$M1/E2$ %	$\alpha_{\rm tot}$	$B(M\lambda)$ (W.u.)
245.0	$7/2^-$	1528(56)	245.0	100	0	$5/2^+$	$E1$		0.012	$1.302(48) \times 10^{-5}$
276.3	$7/2^+$	11.3(34)	276.3	100	0	$5/2^+$	$M1$	79(17)	0.0244	$7.1(26) \times 10^{-2}$
							$E2$	21(17)	0.039	$2.1(18) \times 10^{+2}$
291.4	$3/2^+$	136.5(23)	25.1	0.43(35)	266.3	$1/2^+$	$M1$	$100(^{+0}_{-46})$	[a]	$2.0(^{+17}_{-19}) \times 10^{-2}$
							$E2$	<46		$<1.0 \times 10^{+4}$
			178.0	100(5)	113.4	$1/2^+$	$M1$		0.0776	$1.327(54) \times 10^{-2}$
			291.4	98.6(57)	0	$5/2^+$	$M1$		0.0213	$2.98(13) \times 10^{-3}$
325.3	$3/2^+$	39.6(35)	59.0	2.2(7)	266.3	$1/2^+$	$[M1]$		1.714	$3.9(14) \times 10^{-2}$
			211.9	44(7)	113.4	$1/2^+$	$M1$		0.0488	$1.68(32) \times 10^{-2}$
			325.4	100(19)	0	$5/2^+$	$M1$	$85(^{+15}_{-20})$	0.01611	$8.9(^{+19}_{-24}) \times 10^{-3}$
							$E2$	$15(^{+20}_{-15})$	0.0227	$12(^{+17}_{-12})$
326.8	$5/2^+$	832(27)	35.3	2.4(3)	291.4	$3/2^+$	$M1$	$84(^{+16}_{-29})$	7.65	$8.4(^{+28}_{-50}) \times 10^{-3}$
							$E2$	$16(^{+29}_{-16})$	58.3	$1.1(^{+2.2}_{-1.2}) \times 10^{+3}$
			50.6	0.06(2)	276.3	$7/2^+$	$[M1]$		2.68	$8.5(^{+3.1}_{-3.5}) \times 10^{-5}$
			81.8	1.3(1)	245.0	$7/2^-$	$E1$		0.272	$5.9(^{+10}_{-15}) \times 10^{-6}$
			326.8	100	0	$5/2^+$	$M1$	<23	0.01591	$<1.2 \times 10^{-4}$
							$E2$	$100(^{+0}_{-23})$	0.0223	$4.1(^{+6}_{-14})$
426.1	$7/2^+$	73.6(42)	149.9	8(1)	276.3	$7/2^+$	$[M1]$		0.1237	$6.5(10) \times 10^{-3}$
			426.1	100(10)	0	$5/2^+$	$M1$	$100(^{+0}_{-27})$	0.00822	$3.52(^{+21}_{-97}) \times 10^{-3}$
							$E2$	<27	0.00963	<4.6
491.5	$3/2^+$	62.9(42)	166.3	7(3)	325.3	$3/2^+$	$[M1]$		0.0932	$2.8(12) \times 10^{-3}$
			200.2	45(6)	291.4	$3/2^+$	$M1$	$100(^{+0}_{-3})$	0.0567	$1.02(14) \times 10^{-2}$
							$E2$	<3	0.1183	<6.9
			378.2	100(10)	113.4	$1/2^+$	$[M1]$		0.01104	$3.38(32) \times 10^{-3}$
			491.5	35(5)	0	$5/2^+$	$[M1]$		0.00581	$5.38(80) \times 10^{-4}$
540.6	$5/2^+$	29.3(43)	213.8	9(2)	326.8	$5/2^+$	$[M1]$		0.0476	$3.8(10) \times 10^{-3}$
			215.4	33(4)	325.3	$3/2^+$	$M1$	$100(^{+0}_{-9})$	0.0467	$1.38(^{+26}_{-29}) \times 10^{-2}$
							$E2$	<9	0.0915	<26
			249.2	100(10)	291.4	$3/2^+$	$M1$	$100(^{+0}_{-11})$	0.0319	$2.70(^{+42}_{-52}) \times 10^{-2}$
							$E2$	<11	0.0553	<47
			264.4	7(2)	276.3	$7/2^+$	$M1$	57(35)	0.0274	$9.0(62) \times 10^{-4}$
							$E2$	43(35)	0.0452	8.1(71)
			274.3	2(1)	266.3	$1/2^+$	$E2$		0.0399	4.5(23)
			295.6	6(1)	245.0	$7/2^-$	$E1$		0.00721	$1.31(30) \times 10^{-5}$
			427.3	<5	113.4	$1/2^+$	$E2$		0.00955	<1.6
			540.6	12(4)	0	$5/2^+$	$[M1]$		0.00462	$3.2(11) \times 10^{-4}$

[a]Measured total transition intensity ($I_{\rm tot} = I_\gamma + I_{ce}$); see text.

A. The low-lying $7/2^+$ levels

The two low-lying $7/2^+$ levels appear systematically across the Pd isotopic chain beginning at the $N = 50$ major shell closure and continue into the exotic neutron-rich isotopes. Single-neutron transfer [21,24–29] and high spin studies [41–48] indicate that one of these levels consistently displays a $\nu g_{7/2}$ single-particle character, while the other can be described as a $\nu d_{5/2} \otimes 2^+_1$ configuration. This distinction is based on the observed spectroscopic strengths (Table II) and band structures connected to them (Fig. 5). The exception to this is in ^{107}Pd where the level structures seem to be mixed due to the close proximity in energy of the $7/2^+$ states as well as the isolated

TABLE II. (Color online) Low-lying $\ell = 4$ spectroscopic strengths for odd-mass Pd isotopes. The notation "N/A" means data is not available, "N/I" means the $7/2^+_2$ level has not yet been identified in any experiment, and "N/O" means the level was not observed in the transfer experiment, but was identified through a different type of measurement(s). The colors in the table correspond with those in Figs. 5 and 6. Data taken from the NNDC nuclear database [21].

$^A X_N$	(d,p)		(d,t)	
	$7/2^+_1$	$7/2^+_2$	$7/2^+_1$	$7/2^+_2$
^{101}Pd$_{55}$	N/A	N/A	$\ell = 4, 4.68$	N/I
^{103}Pd$_{57}$	$\ell = 4, 3.82$	$\ell = 2, 0.35$	$\ell = 4, 4.28$	$\ell = 2$
^{105}Pd$_{59}$	N/O	[a]	$\ell = 4, 2.52$ [b]	$\ell = (2), 0.04$ [b]
^{107}Pd$_{61}$	$\ell = 4, 0.26$	$\ell = 4, 0.45$	$\ell = (4), 2.78$	$\ell = (4), 1.82$
^{109}Pd$_{63}$	N/O	$\ell = 4, 1.6$	N/O	$\ell = 4, 4.0$
^{111}Pd$_{65}$	$\ell = 4, 0.14$	N/I	N/A	N/A

[a]Observed, but no assignment made.
[b]From (p,d).

occurrence of a third low-lying $7/2^+$ state in the same vicinity [21,27]. The energy systematics of the two $7/2^+$ states in the Pd isotopes compared to the even-even Pd 2^+_1 levels are shown in Fig. 6. Clearly the two different structures display unique evolutionary trends. The $g_{7/2}$ single-particle state drops abruptly after the $N = 50$ shell closure and maintains a flat trend through ^{105}Pd$_{59}$ before slowly rising beyond that. The $d_{5/2} \otimes 2^+$ state, on the other hand, drops smoothly towards a minimum value around midshell in accordance with the 2^+_1 of the even-even cores. The crossing point of the two structures occurs near ^{107}Pd, which results in the mixed character seen in this nucleus. By ^{109}Pd$_{63}$, the two levels are well separated again, and the distinct structure is evidenced by the neutron transfer strengths [49,50], and confirmed in this work by the lifetime measurements and resulting transition probabilities which are discussed below.

One interesting feature of the Pd isotopes is the apparent consistency in the structure of the $5/2^+$ ground states. Single-neutron transfer experiments indicate a strong $d_{5/2}$ single-particle character of the ground state which persists across the stable Pd isotopes (Table III) [21,24–29]. Although based on Fig. 5, one might expect the pure d-wave character to begin to deteriorate as the ground state quasirotational band begins to exhibit a deformation-aligned character starting near $N = 59$. Nevertheless, the $5/2^+$ ground state has been identified up to $N = 67$ [21,30], and the $\ell = 2$ spectroscopic strengths remain strong at least up to $N = 63$ (Table III).

These facts combined with the trajectory of the $g_{7/2}$ single-particle state are indicative of the following: (1) the $d_{5/2}$ single-particle orbital remains partially filled even when the valence neutron number is much greater than the maximum occupancy of the orbital (i.e., the occupancies of other single-particle orbitals become more energetically favorable for these valence neutrons), (2) $\nu g_{7/2}$ achieves significant occupancy relatively early (by $N = 53$) and seems to be mostly filled by $N = 60$ (Fig. 6), and (3) the unpaired neutrons in the odd-mass Pd isotopes prefer to sit in the $d_{5/2}$ orbital. In fact, (2) is not entirely unexpected since the $\nu g_{7/2}$ is predicted to come down in energy due to the interaction with valence $g_{9/2}$ protons [51,52], and this behavior has already been confirmed experimentally in $N = 51$ isotones [53]. Moreover, the $\pi g_{9/2}$-$\nu g_{7/2}$ interaction had been proposed early on by Federman and Pittel to be responsible for the onset of deformation in the Zr and Mo isotopes [54].

A shape change to large deformation is also evident in the band structure of the odd-mass Pd isotopes [41–48] (Fig. 5) and suggested by $B(E2)$ systematics [21,55–59]. Yet, Stefanova *et al.* [48] have recently suggested a transition to γ softness beyond $N = 61$ which may be maximal at ^{109}Pd$_{63}$ and ^{111}Pd$_{65}$. This makes the transition strengths measured in this work crucial for testing nuclear models. In particular, the $7/2^+$ states, with their differing structures, provide an excellent testing ground since lifetime information has been obtained for both levels in this work, and these can be compared with existing lifetime data for the corresponding states in the stable isotope ^{105}Pd$_{59}$ [26], just prior to the shape change.

A comparison between ^{105}Pd and ^{109}Pd is shown in Table IV. Note that the transition $7/2^+_d \rightarrow 7/2^+_g$ has not been observed in ^{105}Pd, so we roughly estimate an upper limit on the strength based on the weakest observed γ-ray intensities in the 100-keV energy region as measured in ^{105}Ag electron capture experiments [26]. The strengths displayed in the table provide further support of the interpretations discussed above. The intraband transition $7/2^+_d \rightarrow 5/2^+_1$ is relatively enhanced compared with the average $B(M1)$ for even-Z odd-N nuclides in this mass region (0.016 W.u., based on data from Ref. [60]) while the other two transitions are hindered. Such a hindrance is expected from a state with a predominant $\nu g_{7/2}$ configuration to states exhibiting a $\nu d_{5/2}$ character, since both $M1$ and $E2$ transitions would be suppressed (the former could not produce the required $\Delta\ell = 2$ while the latter could not produce the required spin flip between $g_{7/2}$ and $d_{5/2}$). The fourth transition in Table IV between $5/2^+$ states is discussed below. A detailed theoretical investigation is currently underway to ascertain which nuclear shape best reproduces the level energies and new lifetime results.

B. The $7/2^-_1$ level

The $7/2^-$ level at 245 keV is interesting since it seems to be the only negative-parity state which is strongly populated in the β decay of ^{109}Rh (ground state $J^\pi = 7/2^+$). The negative-parity states have been the subject of theoretical investigation in the past since they form an isolated set of levels with common structure originating from the $\nu h_{11/2}$ single-particle orbital [38,61,62]. Indeed, an $11/2^-$ isomer is observed throughout the region with a half-life typically of several minutes. In ^{109}Pd, this isomer occurs at 189 keV.

The $7/2^-$ level at 245 keV has been interpreted as a $\nu h_{11/2} \otimes 2^+$ anti-aligned state, based on particle-rotor model calculations [38]. With this interpretation, one would expect a strong $E2$ transition to the $11/2^-$ band head situated below. However, this transition has not been observed in this experiment or any of the previous experiments due to the hindrance from the energy spacing of the transition and the much faster $E1$ transition to the $5/2^+$ ground state. This has been discussed previously by Casten *et al.* [38], where it was noted that the γ-

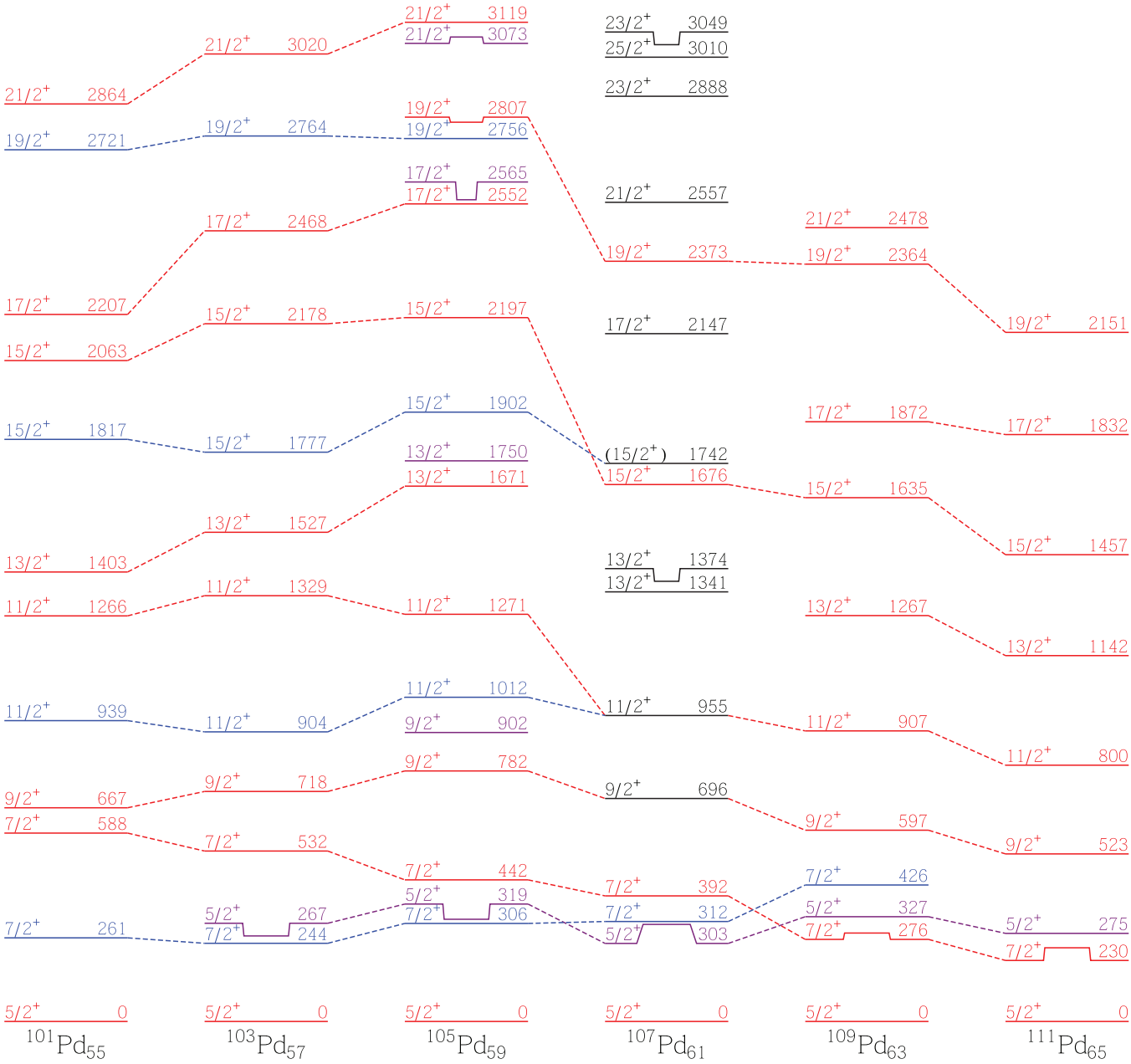

FIG. 5. (Color) The observed band structures in Pd isotopes near $N = 60$. The colors are based on data from Refs. [41–48]. The blue levels are associated with the excited $7/2^+$ band heads while the red levels comprise the $5/2^+$ ground-state bands. In ^{101}Pd the ground-state band transitions start out as $\Delta J = 2$, however $\Delta J = 1$ transitions begin to appear in ^{103}Pd, and by ^{105}Pd a strongly coupled band is well developed. A sudden shape change is apparent at ^{107}Pd at higher spins, however the band assignments are uncertain in this nucleus due to mixing of the low-lying $7/2^+$ states. The purple levels highlight the $5/2_2^+$ states and associated band structure observed in ^{105}Pd [45].

ray intensity would likely fall below the detection threshold for their experiment. This can now be confirmed from the lifetime measurement of the $7/2^-$ level obtained in this study, with $T_{1/2} = 1.528(56)$ ns resulting in $B(E1) = 1.302(48) \times 10^{-5}$ W.u. for the ground-state transition. Assuming a maximum possible $E2$ transition strength of about 40 W.u., which is comparable to the $B(E2, 2_1^+ \rightarrow 0_1^+)$ of the adjacent even-even isotopes ^{108}Pd and ^{110}Pd, the γ-ray intensity of the 56-keV transition to the $11/2^-$ level will be 400 times weaker than the ground-state transition (after conversion-electron correction). This corresponds to 0.03 photons per 1000 β decays [28,37] which is 10 times weaker than the lowest intensity measured by Kanazawa *et al.* [37] and 5 times weaker than the upper limit established in this experiment. The ^{108}Pd(n,γ) study by Casten *et al.* [38] was not sensitive enough either, with an upper limit of 1.5 photons per 1000 neutron captures, while the actual intensity is expected to be about 4 times weaker at 0.4 photons per 1000 neutron captures. Thus, in all cases the experimental limits are consistent with the particle-rotor interpretation.

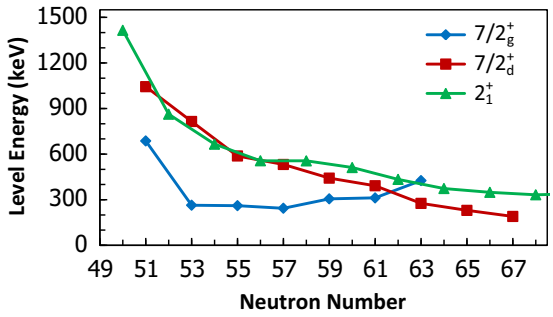

FIG. 6. (Color online) The energies of the two low-lying $7/2^+$ states along with the 2^+_1 of the even-even Pd isotopes are shown as a function of N. The two trends provide additional support for the distinct structure of these levels. The $g_{7/2}$ and $d_{5/2}$ characters are assigned based on earlier neutron-transfer and high-spin measurements. It is seen that both sets of levels exhibit a transition beyond $N = 58$. The $g_{7/2}$ single-particle state begins to rise in energy, indicating a nearly filled occupancy, while the $d_{5/2} \otimes 2^+_1$ state deviates from the 2^+_1 trend, coinciding with the $d_{5/2}$ ground-state band switching from $\Delta J = 2$ to $\Delta J = 1$ [41,43,45]. Data taken from the NNDC nuclear database [21].

However, there have been noted difficulties in the interpretation of the higher-lying, low-spin negative-parity levels [38]. The energies and spacings of these so-called unfavored states (unfavored meaning that the coupled angular momentum between the unpaired neutron and core are neither fully aligned or fully anti-aligned), could not be produced by particle-rotor models using the standard BCS pairing approximation without the aid of an unphysically large Coriolis strength attenuation. However, these states were reproduced quite well in lower mass Pd isotopes using the same model. In particular, the model was successfully applied up to ^{105}Pd [38,63].

Here again is additional evidence of a significant structural change occurring between ^{105}Pd and ^{109}Pd. It was later shown by Henriquez, Rekstad, and England that the particle-rotor model was capable of reproducing the unfavored states in ^{109}Pd with a proper treatment of the pairing interaction using the particle plus recoil (PPR) model [62]. They found that the degree of Coriolis attenuation is dependent on the structure at the Fermi surface. The attenuation is less pronounced when the Fermi surface is spread across orbitals originating from the same spherical parentage as compared to the case when it includes a mixture of orbital structures. This is due to the blocking of occupation of the high-Ω orbitals by the unpaired neutron due to the selection rules of the recoil term of the rotor Hamiltonian [64] which reduces the diffuseness of the pairing distribution. As a result, the total number of Coriolis matrix elements is decreased, effectively quenching the overall interaction strength.

TABLE IV. Strengths for transitions (W.u.) involving lowest $7/2^+$ and $5/2^+$ levels in ^{105}Pd$_{59}$ [26] and ^{109}Pd$_{63}$ (this work).

Transition	$^{105}_{46}$Pd$_{59}$		$^{109}_{46}$Pd$_{63}$	
	$B(M1)$	$B(E2)$	$B(M1)$	$B(E2)$
$7/2^+_g \rightarrow 5/2^+_1$	<0.011	<0.3	0.00351^{+21}_{-97}	<4.6
$7/2^+_d \rightarrow 5/2^+_1$	0.065(24)	15(6)	0.071(26)	$2.1(18)\times10^2$
$7/2^+_d \rightarrow 7/2^+_g$	$\lesssim$0.005		<0.0065(10)	
$5/2^+_2 \rightarrow 5/2^+_1$	0.016(2)	1.5(2)	<0.00012	$4.1(^{+6}_{-14})$

This interpretation suggests a change in the purity of the orbitals at the Fermi surface between ^{105}Pd and ^{109}Pd. Such a change, of course, would be instigated by the sudden increase in deformation which appears to occur here (Fig. 5). The evolution of level energies and neutron-transfer strengths suggests an occupancy predominantly limited to $d_{5/2}$ and $g_{7/2}$ orbitals for ^{105}Pd$_{59}$ and lighter isotopes as discussed above, while for ^{109}Pd$_{63}$ and heavier isotopes the level systematics indicate a more complicated Fermi surface polluted by $s_{1/2}$ and $h_{11/2}$ orbitals (Fig. 7). This would provide a consistent picture for the extra Coriolis attenuation needed in ^{109}Pd as well as the observed $7/2^+$ systematics discussed above and the behavior of the $5/2^+_2$ level discussed next.

C. The $5/2^+_2$ level

The $5/2^+_2$ levels in the Pd isotope chain show particularly interesting behavior. In plotting the energies of this level as a function of neutron number, one finds a sharp drop in energy at $N = 57$, immediately followed by a smooth, flat trend as far as the experimental data exists (Fig. 8). The most striking feature is the enhanced β feeding to this level from $7/2^+$ odd-Z parents, which only exist beginning precisely at $N = 56$. Below $N = 56$, odd-mass Pd isotopes are fed by $9/2^+$ Ag

TABLE III. Low-lying $\ell = 2$ spectroscopic strengths for odd-mass Pd isotopes. The notation "N/A" means data is not available and "N/I" means the $5/2^+_2$ level has not yet been identified in any experiment. Data taken from the NNDC nuclear database [21].

^AX_N	(d,p)		(d,t)	
	$5/2^+_1$	$5/2^+_2$	$5/2^+_1$	$5/2^+_2$
^{101}Pd$_{55}$	N/A	N/A	$\ell = 2, 2.43$	N/I
^{103}Pd$_{57}$	$\ell = 2, 2.96$	$\ell = 2, 0.08$	$\ell = 2, 2.09$	$\ell = 2, 0.21$
^{105}Pd$_{59}$	$\ell = 0$	$\ell = (0 + 2 + 4)$[a]	$\ell = 2, 1.78$[b]	$\ell = 2, 0.36$ [b]
^{107}Pd$_{61}$	$\ell = 2, 0.21$	$\ell = 2, 0.10$	$\ell = 2, 1.39$	$\ell = 2, 0.16$
^{109}Pd$_{63}$	$\ell = 2, 1.06$	$\ell = (2,0), (0.18,0.018)$	$\ell = 2, 1.16$	$\ell = 2, 0.063$
^{111}Pd$_{65}$	$\ell = 2, 0.13$	N/I	N/A	N/A

[a]From (d,t).
[b]From (p,d).

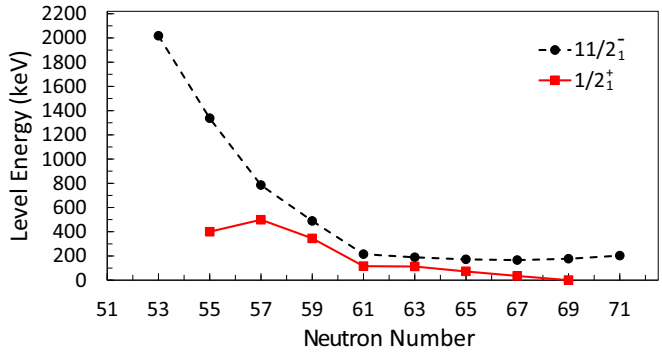

FIG. 7. (Color online) Energies for the $11/2_1^-$ and $1/2_1^+$ levels in Pd isotopes. By $N = 61$, both levels appear to play a prominent role in the structure of the Fermi surface. Data taken from the NNDC nuclear database [21].

parents. The log ft values for decays to this level from the $7/2^+$ parents (consisting of both Ag and Rh) range between 5.2 and 4.8 (Table V), putting them firmly in the enhanced side for allowed β decays. This suggests that these $5/2_2^+$ states are closely related to the $7/2^+$ ground states of the Ag and Rh parents.

These $7/2^+$ states in Ag and Rh are an example of the well-known $I = j - 1$ anomaly, and have been described as higher seniority ($\nu = 3$) $(\pi g_{9/2})^3$ configurations [65,66]. The connection between these states and the $5/2_2^+$ states in the Pd daughters has been pointed out more recently by Lhersonneau *et al.* [14,67]. Examining the systematics of these $7/2^+$ states relative to their $\nu = 1$, $9/2^+$ counterparts in the Rh and Ag isotopic chains (Fig. 8), it is seen that the $7/2^+$ configuration becomes the favored one at $N = 56$ in Ag and $N = 58$ in Rh, giving rise to this configuration in the Pd daughters at $N = 57$ (where Ag is initially the parent switching over to Rh as the stability line is crossed). This, combined with the characteristic low log ft values, identifies these $5/2_2^+$ states as

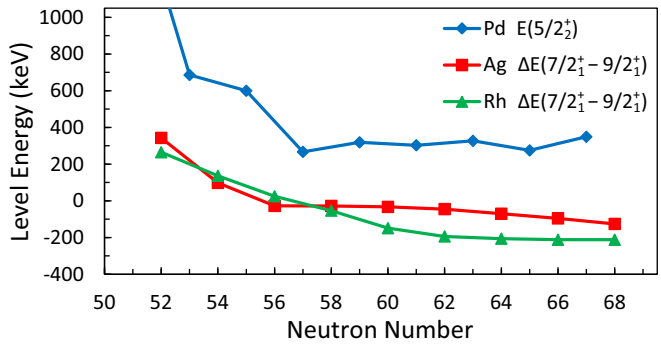

FIG. 8. (Color online) Energies of the $5/2_2^+$ levels in Pd isotopes (blue diamonds) are shown as a function of N. Also plotted are the energies of the $7/2_1^+$ levels relative to the $9/2_1^+$ levels in Ag (red squares) and Rh (green triangles) isotopes. The correlation between $5/2_2^+$ in Pd and $7/2_1^+$ in Ag and Rh is evident. Once the $7/2^+$ becomes favored over the $9/2^+$ in Ag, the $5/2_2^+$ level in the Pd daughters changes significantly (see also Table V). Data taken from the NNDC nuclear database [21].

TABLE V. β decays from Ag and Rh parents to the $5/2_2^+$ level in Pd daughters. Data taken from Nuclear Data Sheets, Refs. [21,23–30].

^{A}Pd$_N$	$E(5/2_2^+)$ keV	Parent, J^π	log ft
^{99}Pd$_{53}$	686	^{99}Ag, $(9/2)^+$	6.58(9)
^{101}Pd$_{55}$	600	^{101}Ag, $9/2^+$	
^{103}Pd$_{57}$	267	^{103}Ag, $7/2^+$	5.25(5)
^{105}Pd$_{59}$	319	^{105}Rh, $7/2^+$	5.112(21)
^{107}Pd$_{61}$	303	^{107}Rh, $7/2^+$	5.0(1)
^{109}Pd$_{63}$	327	^{109}Rh, $7/2^+$	4.82(7)
^{111}Pd$_{65}$	275	^{111}Rh, $(7/2^+)$	
^{113}Pd$_{67}$	349	^{113}Rh, $(7/2^+)$	4.93(4)

a three-quasiparticle configuration of $[(\pi g_{9/2})^2,(\nu g_{7/2})^1]_{5/2+}$, where the low log ft is explained by the Gamow-Teller decay of a paired $g_{7/2}$ neutron (in the case of Rh) into a $g_{9/2}$ proton leaving an unpaired $g_{7/2}$ neutron and a $\nu = 2$ set of $g_{9/2}$ protons (in Ag parents an unpaired $g_{9/2}$ proton decays to a $g_{7/2}$ neutron).

The lifetime of this state in ^{109}Pd was measured in the present work. The multipolarity of the transition between this state and the ground state was determined to be pure $E2$ by Casten *et al.* [38], which is expected for a $\nu = 2$ to $\nu = 0$ transition. This results in a reduced transition strength of $B(E2) = 4.1(^{+06}_{-14})$ W.u.. An upper limit on the $M1$ strength set by Ref. [38] results in $B(M1) < 0.0012$ W.u.. As with the $7/2^+$ states, this can be compared to the corresponding state in ^{105}Pd which has lifetime information [26] (Table IV). Interestingly, the lifetime of this state in ^{105}Pd is much shorter due to a strong $M1$ component in the transition to the ground state. The resulting transition strengths are $B(E2) = 1.5(2)$ W.u. and $B(M1) = 0.016(2)$ W.u. for the 319-keV $5/2_2^+ \rightarrow 5/2_1^+$ transition.

The fact that the $M1$ and $E2$ strengths differ by so much from $N = 59$ to $N = 63$ is interesting considering that both $5/2_2^+$ states exhibit the same behavior, i.e., strong β feeding from $7/2^+$ Rh parents with similar log ft values and excitation energies. Moreover, the $5/2^+$ Pd ground states that these deexcite to appear to maintain strong $d_{5/2}$ single-particle structure (evident from neutron-transfer strengths) as mentioned earlier, although ^{109}Pd may have increased $\ell = 4$ admixture due to larger deformation (Fig. 5). Another possible complication is admixture in ^{105}Pd from a signature of the $\nu g_{7/2}$ band, as suggested by the results of Rickey *et al.* [45] (see also Fig. 5). However, it is not qualitatively obvious how the $M1$ and $E2$ transition strengths should be affected by such admixtures. It would be interesting to measure the lifetimes of these states across a large isotopic range to see how the $M1$ and $E2$ strengths evolve. It is possible that this lifetime in either ^{105}Pd or ^{109}Pd is an anomaly, but it could be that the $M1$ strength persists up to the $N = 60$ shape change, where it suddenly vanishes. A quantitative theoretical investigation on this would also be interesting.

The $5/2_2^+$ levels in Pd isotopes at $N \geqslant 57$ are most interesting because they highlight the onset of a dominance of p-n interactions over pairing interactions. In the Federman and Pittel work [54] referenced earlier, the onset of deformation

near $N = 60$ is attributed to p-n interactions between valence nucleons in the spin-orbit partner orbitals $\pi g_{9/2}$ and $\nu g_{7/2}$ which are filling simultaneously in this region. The deformation arises when such interactions begin to dominate the spherical-favoring p-p and n-n pairing interactions. A more recent investigation of such p-n interactions has been provided by Otsuka *et al.* [51,52], where the tensor component of the monopole force was identified as a key factor in the strength of the interaction. The interaction strength is expected to increase with the filling of both orbitals. Experimental evidence of this was later provided by Sharp *et al.* [53].

Such a dominance of the p-n interactions is perhaps even more explicit in the Rh, Pd, and Ag isotopes as increased seniority configurations start to become favorable. As Z increases beyond 45, $\pi g_{9/2}$ becomes greater than half occupied, which increases the binding of $g_{7/2}$ neutrons. This would help explain the early occupancy of $g_{7/2}$ before filling $d_{5/2}$ in Pd isotopes and also why the $7/2^+$ ground state first appears at lower N in Ag compared to Rh (Fig. 8). A further consequence of this strong p-n interaction is the inversion of $\pi p_{1/2}$ and $\pi g_{9/2}$ in this region due to the increased binding energy of the latter. Experimental evidence for this and its possible influence on ground-state shape evolution has been discussed in Ref. [36].

V. SUMMARY AND CONCLUSIONS

A study of subnanosecond lifetimes of excited states in odd-mass neutron-rich nuclides in the mass region $A \sim 110$ is underway. The results from the measurement involving levels in ^{109}Pd are presented in this paper. The good timing characteristics of the plastic and $LaBr_3$(Ce) scintillation detectors allowed for precise lifetime measurements down to $\sim$10 ps.

The new lifetimes, when combined with the already existing nuclear data, provide insight to the microscopic nuclear structure governing the mass region, bolstering formerly proposed theoretical assertions. Of particular interest are the low-lying $7/2^+$ and $5/2^+$ states which occur systematically across the Pd isotopes. The characteristics of these levels provide additional evidence of a strong interaction between valence $g_{9/2}$ protons and $g_{7/2}$ neutrons which may drive the evolution of bulk nuclear properties within this mass region, such as the apparent onset of deformation at $N = 60$. The new lifetimes measured here provide the transition rates between these relevant states, which add an important constraint for nuclear models. The present work provides motivation for a detailed theoretical study to try to understand quantitatively this strong p-n interaction and how it influences phenomena such as higher seniority configurations, shape transitions, and movements of single-particle orbitals. Theoretical efforts investigating the nuclear shape transition in the Pd isotopes is currently being pursued by comparing the available experimental data with calculations using geometric particle-rotor models. A detailed understanding of the underlying nuclear structure and how it evolves is necessary for reliable predictions of nuclear input for r-process and nucleosynthesis studies.

In conclusion, a thorough consideration of much of the available experimental data in the neutron-rich Pd isotopes has identified a number of interesting nuclear structure effects, all occurring near $N = 58$–60. The present discussion has been focused on the lowest $5/2^+$ and $7/2^+$ states. The new lifetime measurements provided in this work complement the other available experimental data including neutron-transfer strengths, rotational-band assignments, and β-decay properties. These, along with level energies, spins, and parities in the surrounding nuclei, help to characterize the shape transition at $N = 60$ for the Pd isotopes. All the structure effects discussed above seem to be correlated and are likely driven by the p-n interaction between valence $g_{9/2}$ protons and $g_{7/2}$ neutrons. A detailed understanding of such effects and how they evolve along the nuclear landscape will be of great importance for reliable predictions of nuclear properties for the r-process and subsequent nucleosynthesis calculations. In particular, the migration of the high-j, unique parity $\pi g_{9/2}$ orbital may induce isomerism along with a potentially strong influence on β-decay lifetimes. Additionally, such rapid shape changes, like the one at $N = 60$, could affect nuclear masses, neutron-capture cross sections, as well as β-decay lifetimes [68,69], potentially influencing r-process dynamics.

ACKNOWLEDGMENTS

B.B. would like to acknowledge helpful discussions with S. Frauendorf and A. O. Macchiavelli. Figures 1(a), 4, and 5 were created using the LEVELSCHEME scientific figure preparation system [70]. This project was funded by the National Science Foundation through Grants No. PHY0822648 and No. PHY0758100 and supported by EU 6th Framework program (Integrating Infrastructure Initiative–Transnational Access) Contract No. 506065 (EURONS), the Spanish MINECO via FPA-2013-41267-P, and by the Academy of Finland under the Centre of Excellence Programme 2006-2011 (nuclear and accelerator based physics program at JYFL). B.B. acknowledges support from the U.S. Department of Energy and Lawrence Livermore National Laboratory under Contract No. DE-AC52-07NA27344.

[1] K. Heyde and J. L. Wood, Rev. Mod. Phys. **83**, 1467 (2011).
[2] J. A. Pinston, W. Urban, C. Droste, T. Rzaça-Urban, J. Genevey, G. Simpson, J. L. Durell, A. G. Smith, B. J. Varley, and I. Ahmad, Phys. Rev. C **74**, 064304 (2006).
[3] A. M. Bruce, S. Lalkovski, A. M. Denis Bacelar, M. Górska, S. Pietri, Z. Podolyák, Y. Shi, P. M. Walker, F. R. Xu *et al.*, Phys. Rev. C **82**, 044312 (2010).
[4] B. Sorgunlu and P. Van Isacker, Nucl. Phys. A **808**, 27 (2008).

[5] M. Böyükata, P. Van Isacker, and İ. Uluer, J. Phys. G **37**, 105102 (2010).
[6] J. Rogowski, N. Kaffrell, D. De Frenne, K. Heyde, E. Jacobs, M. Harakeh, J. Schippers, and S. Van Der Werf, Phys. Lett. B **207**, 125 (1988).
[7] J. Kurpeta, J. Rissanen, A. Płochocki, W. Urban, V.-V. Elomaa, T. Eronen, J. Hakala, A. Jokinen, A. Kankainen *et al.*, Phys. Rev. C **82**, 064318 (2010).
[8] G. Simpson, J. Genevey, J. A. Pinston, U. Köster, R. Orlandi, A. Scherillo, and I. A. Tsekhanovich, Phys. Rev. C **75**, 027301 (2007).
[9] J. Äystö, P. P. Jauho, Z. Janas, and A. Jokinen, Nucl. Phys. A **515**, 365 (1990).
[10] J. Kurpeta, W. Urban, A. Płochocki, J. Rissanen, V.-V. Elomaa, T. Eronen, J. Hakala, A. Jokinen, A. Kankainen *et al.*, Phys. Rev. C **82**, 027306 (2010).
[11] J. Kurpeta, W. Urban, A. Płochocki, J. Rissanen, J. A. Pinston, V.-V. Elomaa, T. Eronen, J. Hakala, A. Jokinen *et al.*, Phys. Rev. C **86**, 044306 (2012).
[12] S. Lalkovski, A. Minkova, M.-G. Porquet, A. Bauchet, I. Deloncle, A. Astier, N. Buforn, L. Donadille, O. Dorvaux *et al.*, Eur. Phys. J. A **18**, 589 (2003).
[13] M. Varshney, M. Singh, Y. Singh, C. Bihari, A. K. Varshney, K. K. Gupta, and D. K. Gupta, Phys. Scr. **83**, 015201 (2011).
[14] G. Lhersonneau, B. Pfeiffer, J. Alstad, P. Dendooven, K. Eberhardt, S. Hankonen, I. Klöckl, K.-L. Kratz, A. Nähler *et al.*, Eur. Phys. J. A **1**, 285 (1998).
[15] P. Regan, C. Beausang, N. Zamfir, R. Casten, J.-y. Zhang, A. Yamamoto, M. Caprio, G. Gürdal, A. Hecht *et al.*, Phys. Rev. Lett. **90**, 152502 (2003).
[16] R. M. Clark, P. Fallon, A. Görgen, M. Cromaz, M. A. Deleplanque, R. M. Diamond, G. J. Lane, I. Y. Lee, A. O. Macchiavelli, R. G. Ramos, F. S. Stephens, C. E. Svensson, K. Vetter, D. Ward, M. P. Carpenter, R. V. F. Janssens, and R. Wadsworth, Phys. Rev. Lett. **87**, 202502 (2001).
[17] M. Quinn, A. Aprahamian, J. Pereira, R. Surman, O. Arndt, T. Baumann, A. Becerril, T. Elliot, A. Estrade, D. Galaviz, T. Ginter, M. Hausmann, S. Hennrich, R. Kessler, K.-L. Kratz, G. Lorusso, P. F. Mantica, M. Matos, F. Montes, B. Pfeiffer, M. Portillo, H. Schatz, F. Schertz, L. Schnorrenberger, E. Smith, A. Stolz, W. B. Walters, and A. Wöhr, Phys. Rev. C **85**, 035807 (2012).
[18] H. Mach and L. M. Fraile, Hyperfine Interact. **223**, 147 (2014).
[19] M. Sanchez-Vega, H. Mach, R. B. E. Taylor, B. Fogelberg, A. Lindroth, A. J. Aas, P. Dendooven, A. Honkanen, M. Huhta *et al.*, Eur. Phys. J. A **35**, 159 (2008).
[20] D. Smith, H. Mach, H. Penttilä, H. Bradley, J. Äystö, V.-V. Elomaa, T. Eronen, D. Ghiţă, J. Hakala *et al.*, Phys. Rev. C **77**, 014309 (2008).
[21] Brookhaven National Laboratory, NNDC nuclear database, http://www.nndc.bnl.gov/, accessed May 2013.
[22] N. Nica, Nucl. Data Sheets **111**, 525 (2010).
[23] E. Browne and J. Tuli, Nucl. Data Sheets **112**, 275 (2011).
[24] J. Blachot, Nucl. Data Sheets **83**, 1 (1998).
[25] D. De Frenne, Nucl. Data Sheets **110**, 2081 (2009).
[26] D. De Frenne and E. Jacobs, Nucl. Data Sheets **105**, 775 (2005).
[27] J. Blachot, Nucl. Data Sheets **109**, 1383 (2008).
[28] J. Blachot, Nucl. Data Sheets **107**, 355 (2006).
[29] J. Blachot, Nucl. Data Sheets **110**, 1239 (2009).
[30] J. Blachot, Nucl. Data Sheets **111**, 1471 (2010).
[31] J. Äystö, Nucl. Phys. A **693**, 477 (2001).
[32] P. Karvonen, I. D. Moore, T. Sonoda, T. Kessler, H. Penttilä, K. Peräjärvi, P. Ronkanen, and J. Äystö, Nucl. Instrum. Methods B **266**, 4794 (2008).
[33] H. Mach, R. L. Gill, and M. Moszyński, Nucl. Instrum. Methods A **280**, 49 (1989).
[34] M. Moszyński and H. Mach, Nucl. Instrum. Methods **A277**, 407 (1989).
[35] H. Mach, F. K. Wohn, G. Molnar, K. Sistemich, J. C. Hill, M. Moszyński, R. L. Gill, W. Krips, and D. S. Brenner, Nucl. Phys. A **523**, 197 (1991).
[36] B. Bucher, Ph.D. Thesis, University of Notre Dame, 2014.
[37] M. Kanazawa, S. Ohya, T. Tamura, Z.-i. Matumoto, and N. Mutsuro, J. Phys. Soc. Jpn. **44**, 25 (1978).
[38] R. F. Casten, G. J. Smith, M. R. Macphail, D. Breitig, W. R. Kane, M. L. Stelts, S. F. Mughabghab, J. A. Cizewski, H. G. Börner *et al.*, Phys. Rev. C **21**, 65 (1980).
[39] T. Kibédi, T. W. Burrows, M. B. Trzhaskovskaya, P. M. Davidson, and C. W. Nestor, Nucl. Instrum. Methods A **589**, 202 (2008), http://bricc.anu.edu.au/.
[40] P. Fettweis and P. del Marmol, Z. Phys. A **275**, 359 (1975).
[41] P. C. Simms, G. J. Smith, F. A. Rickey, J. A. Grau, J. R. Tesmer, and R. M. Steffen, Phys. Rev. C **9**, 684 (1974).
[42] R. Popli, F. A. Rickey, and P. C. Simms, Phys. Rev. C **22**, 1121 (1980).
[43] J. A. Grau, F. A. Rickey, G. J. Smith, P. C. Simms, and J. R. Tesmer, Nucl. Phys. A **229**, 346 (1974).
[44] B. M. Nyakó, J. Gizon, A. Gizon, J. Timár, L. Zolnai, A. J. Boston, D. T. Joss, E. S. Paul, A. T. Semple *et al.*, Phys. Rev. C **60**, 024307 (1999).
[45] F. A. Rickey, J. A. Grau, L. E. Samuelson, and P. C. Simms, Phys. Rev. C **15**, 1530 (1977).
[46] K. R. Pohl, P. H. Regan, J. E. Bush, P. E. Raines, D. P. Balamuth, D. Ward, A. Galindo-Uribarri, V. P. Janzen, S. M. Mullins, and S. Pilotte, Phys. Rev. C **53**, 2682 (1996).
[47] S. Juutinen, P. Šimeček, C. Fahlander, R. Julin, J. Kumpulainen, A. Lampinen, T. Lönnroth, A. Maj, S. Mitarai *et al.*, Nucl. Phys. A **577**, 727 (1994).
[48] E. A. Stefanova, S. Lalkovski, A. Korichi, T. Kutsarova, A. Lopez-Martens, F. R. Xu, H. L. Liu, S. Kisyov, A. Minkova *et al.*, Phys. Rev. C **86**, 044302 (2012).
[49] B. L. Cohen, J. B. Moorhead, and R. A. Moyer, Phys. Rev. **161**, 1257 (1967).
[50] R. C. Diehl, B. L. Cohen, R. A. Moyer, and L. H. Goldman, Phys. Rev. C **1**, 2086 (1970).
[51] T. Otsuka, T. Suzuki, R. Fujimoto, H. Grawe, and Y. Akaishi, Phys. Rev. Lett. **95**, 232502 (2005).
[52] T. Otsuka, T. Suzuki, M. Honma, Y. Utsuno, N. Tsunoda, K. Tsukiyama, and M. Hjorth-Jensen, Phys. Rev. Lett. **104**, 012501 (2010).
[53] D. K. Sharp, B. P. Kay, J. S. Thomas, S. J. Freeman, J. P. Schiffer, B. B. Back, S. Bedoor, T. Bloxham, J. A. Clark *et al.*, Phys. Rev. C **87**, 014312 (2013).
[54] P. Federman and S. Pittel, Phys. Rev. C **20**, 820 (1979).
[55] D. De Frenne, Nucl. Data Sheets **110**, 1745 (2009).
[56] J. Blachot, Nucl. Data Sheets **108**, 2035 (2007).
[57] D. De Frenne and A. Negret, Nucl. Data Sheets **109**, 943 (2008).
[58] J. Blachot, Nucl. Data Sheets **91**, 135 (2000).
[59] G. Gürdal and F. Kondev, Nucl. Data Sheets **113**, 1315 (2012).
[60] P. M. Endt, At. Data Nucl. Data Tables **26**, 47 (1981).

[61] G. J. Smith, R. F. Casten, M. L. Stelts, H. G. Börner, W. F. Davidson, and K. Schreckenbach, Phys. Lett. B **86**, 13 (1979).
[62] A. Henriquez, T. Engeland, and J. Rekstad, Phys. Rev. C **27**, 1302 (1983).
[63] H. Smith and F. Rickey, Phys. Rev. C **14**, 1946 (1976).
[64] J. Rekstad and T. Engeland, Phys. Lett. B **89**, 316 (1980).
[65] V. Paar, Phys. Lett. B **39**, 587 (1972).
[66] V. Paar, Nucl. Phys. A **211**, 29 (1973).
[67] G. Lhersonneau, J. C. Wang, S. Hankonen, P. Dendooven, P. Jones, R. Julin, and J. Äystö, Phys. Rev. C **60**, 014315 (1999).
[68] A. Aprahamian, K. Langanke, and M. Wiescher, Prog. Part. Nucl. Phys. **54**, 535 (2005).
[69] H. Schatz, A. Aprahamian, J. Görres, M. Wiescher, T. Rauscher, J. F. Rembges, F.-K. Thielemann, B. Pfeiffer, P. Möller *et al.*, Phys. Rep. **294**, 167 (1998).
[70] M. A. Caprio, Comput. Phys. Commun. **171**, 107 (2005), http://scidraw.nd.edu/levelscheme.